Premier Journal of Engineering and Applied Sciences
Publication of Nigerian Society of Engineers, Ibadan Branch
P J E A S
Vol. 6, No. 3, 2025 ISSN:2734-3170

Optimizing the Mechanical Properties of Sisal Fiber-Reinforced Self-Compacting Mortar Incorporated with Glass Powder

M. A. Akinpelu, W. A. Ajibowu*, A. M. Salman, A. G. Abdullah, A. B. Olahan and A. A. Olayiwola

Department of Civil and Environmental Engineering, Kwara State University, Malete, Nigeria

***Corresponding Author:** *ajibowuwasiu123@gmail.com*

ARTICLE INFO

Received: May, 2025
Accepted: July, 2025
Published: July, 2025

Keywords:
Glass powder
Mechanical properties
Self-compacting mortar
Sisal fiber

ABSTRACT

Sustainable alternatives are needed to reduce cement use while maintaining self-compacting behavior and enhancing toughness, ductility, and durability. Sisal fiber (SF), with its tensile strength and crack-bridging ability, improves ductility, while recycled glass powder (GP), with pozzolanic properties, reduces cement use and densifies the matrix. Their combined effects in self-compacting mortar (SCM) remain underexplored. This study employs Central Composite Design (CCD) in Design Expert software to optimize SCM mixes with GP replacing cement at 0–22.5% and SF added at 0–1% by volume. Specimens (50 mm cubes and 40 × 40 × 160 mm beams) were tested for mechanical properties at 90 days. Results show that SF enhances both compressive and flexural strength, particularly when combined with GP. The optimal mix containing 7.5% GP and 0.5% SF achieved 37.8 MPa compressive strength and 7.2 MPa flexural strength, representing increases of 12.4% and 18.6%, respectively, over the control. Microstructural analysis confirms dense C–S–H gel formation and improved pozzolanic activity. These findings highlight the potential of GP–SF blends for developing high-performance, eco-friendly self-compacting mortars.

1. INTRODUCTION

Self-compacting mortar (SCM) is a highly flowable, non-segregating mortar that spreads into place and fills formwork without the need for mechanical compaction (Nécira and Abadou, 2021). This type of mortar has properties similar to self-compacting concrete (SCC) but is used in applications where a more refined mixture is required, such as for smaller sections, repairs, or when precise filling of voids is necessary. The construction industry has been a primary focus of research, particularly in concrete technology. The growing demand for urban infrastructure has prompted increased development activities around the world, greatly increasing demand for concrete (Asonibare *et al.*, 2025; Olorunfemi *et al.*, 2025). However, this demand poses a significant environmental risk due to high levels of greenhouse gas emissions, particularly carbon dioxide. To solve this, using industrial waste materials in construction has gained popularity as a way to create greener and more sustainable building materials.

Recycling glass trash can help address some of the challenges connected with glass manufacturing, but the technique is not completely sustainable or cost-effective. Using glass powder (GP) in concrete manufacturing has various issues, including maintaining uniform particle size distribution, assuring consistent levels of purity and quality from recycled sources, and generating appropriate mix designs through rigorous testing (Naran *et al.*, 2022). Long-term durability testing, particularly under difficult

conditions, is critical because concrete experiences several simultaneous effects that have not been well evaluated in real-world contexts. To address these issues, over the last decade, several recycling processes have been used to repurpose waste glass, and its prospective applications in the construction industry, notably in concrete, are being intensively investigated (Tijani *et al.*, 2025; Olofinnade *et al.*, 2017).

Sisal fiber (SF) is a natural reinforcement and viable alternative to synthetic reinforcements due to its high tensile strength, lightweight nature, and biodegradability (More and Subramanian, 2022). When SF is used in SCM, it increases ductility, tensile strength, and energy absorption, improving the material's overall performance. In addition to SF, GP is being recognised as an effective supplemental cementitious material that can partially replace Portland cement in certain circumstances (Rodier and Savastano, 2018). Several studies have been conducted on sustainable materials in SCM. Hammat *et al.* (2021) studied how natural pozzolana (NP) affects the rheological, strength, shrinkage, and water absorption qualities of SCM. The results showed that higher NP content and fineness lowered flowability while increasing long-term strength. Increased NP fineness improved strength while increasing both total and autogenous shrinkage. Higher NP concentration increased water absorption; however, finer NP lowered it marginally.

Horsakulthai (2021) investigated the chemical composition of recycled concrete powder (RCP) and how it affects the physical qualities of SCM. Results showed RCP had a strength-activity index of 89.4% (7 days) and 87.2% (28 days). Increasing RCP content raised porosity and water absorption while reducing resistivity. The optimal RCP replacement for minimal strength loss was 20%. Bentlemsan *et al.* (2023) investigated the use of marble waste fine particles (MW) as an alternative to natural sand in SCM. Results indicate that up to 50% sand replacement maintains good workability and flow time. At 30% and 50% replacement, compressive and flexural strengths increase by 90 days, while porosity decreases at 30%. Mortars with up to 50% MW replacement also showed improved resistance to sulfate attack after 180 days. Scanning electron microscopy (SEM) and energy dispersive spectrum (EDS) analyses detected no significant ettringite formation.

Sara *et al.* (2023) investigated the use of recycled concrete sand (RCS) as a substitute for natural sand and granulated slag (GS) as a cement replacement in SCM production. The results show that SCM can be effectively produced with up to 50% RCS. Although RCS increases porosity and water absorption, these effects can be mitigated by using GS. A 20% GS replacement also improves long-term compressive strength. Souza *et al.* (2023) investigated the use of superabsorbent polymers (SAP) in SCM to control shrinkage and analyze thermal and mechanical properties, aiming for optimal material proportions for large-volume structures. SCM mixes with 0%, 0.1%, and 0.2% SAP were tested with Portland composite cement under dry and submerged curing. Results showed SAP reduced temperature variation, suggesting its potential to mitigate thermal spikes in large structures.

Optimization involves finding the action that best achieves a desired goal or objective, typically by maximizing or minimizing the value of an objective function (Maraghechi *et al.*, 2014). Optimization is an important idea in human affairs because it represents the desire to attain the best possible outcome in any given scenario. There are various optimization techniques, such as linear programming, convex programming, multi-local programming, genetic algorithms, interactive optimization, and response surface methodology (RSM) (Byrne, 2014). Despite the growing body of research on sustainable SCM, few studies have simultaneously investigated the combined influence of natural fibers and recycled GP on both mechanical and microstructural performance. Most existing works have focused on single additives, such as pozzolanic materials or fibers, without optimizing their interaction effects on flowability, strength, and durability.

Moreover, limited studies have applied statistical optimization techniques like the Central Composite Design (CCD) to determine the precise synergy between SF and GP content in SCM. Consequently, the optimal balance that maximizes strength and sustainability while preserving self-compacting behavior remains inadequately defined. This study looks at how SF reinforcement and GP affect the mechanical

properties of SCM. The study's goal is to investigate the mechanical properties of SCM with GP, analyse microstructural changes, and optimize mix proportions for maximum performance and sustainability. Recycling glass into powder saves cement consumption, CO_2 emissions, and trash management, while also providing financial benefits such as lower prices and greater performance.

2. METHODOLOGY

2.1 Materials

Materials employed in this research are Portland limestone cement, fine aggregate, drinkable water, and waste glass. The cement was purchased from Mohadis Construction Limited in Ilorin, Nigeria, while the fine aggregate was sourced from the Asa River in Ilorin. The blend contained potable water that met BS EN 1008 (2002) standards. The discarded glass was collected from restaurants and converted into powder making it waste GP. The GP was then ground to a particle size of 120 microns, and sieved through a 90-micron mesh to ensure uniform particle size. The SF were sourced from agricultural processing facilities in Ilorin, Nigeria, for their high tensile strength, durability, and resistance to moisture. The fibers underwent cleaning, sun-drying, and cutting to uniform lengths to ensure consistent dispersion and bonding within the mortar matrix.

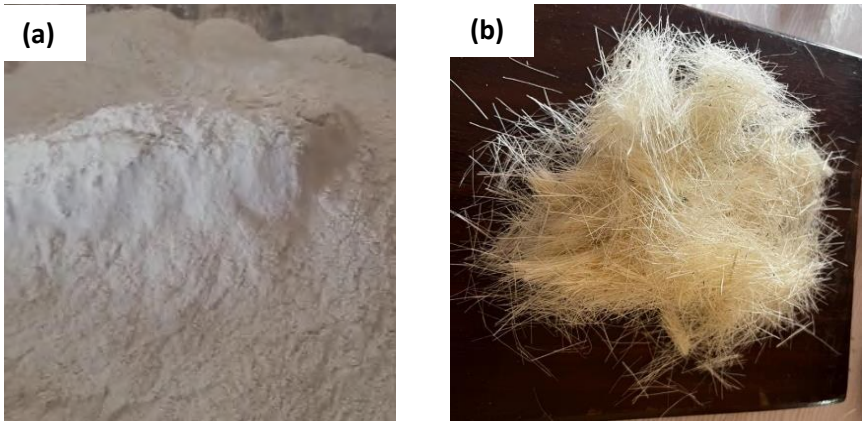

Figure 1: (a) Glass powder (b) Sisal fiber

2.2 Mix proportioning

The mix design in this study was structured to systematically investigate the combined effects of GP and SF content on mortar properties, using the CCD in Design Expert software. Across all 12 mixes (M1–M12), the total binder content was maintained constant, while varying proportions of GP replaced cement at levels of 0, 7.5, 15, and 22.5%. SF content was also varied by volume across three levels: 0, 0.5, and 1%. While cement and GP quantities changed based on the designed replacement ratios, the sand quantity and water volume remained constant for all mixes, allowing the study to isolate and assess the specific influence of GP and SF content. This deliberate variation created a balanced and statistically sound matrix suitable for response surface analysis, enabling the prediction and optimization of mortar performance based on GP and SF incorporation.

To evaluate the strengths of the mortar, three cube specimens with dimensions of 50 × 50 × 50 mm were prepared for compressive strength testing, while three prismatic beams measuring 40 × 40 × 160 mm were cast for flexural strength assessment. All specimens were compacted with a mechanical vibration table to guarantee appropriate consolidation. After casting, they were kept for 24 hours. After this interval, the specimens were demoulded and placed in water at 27°C for curing. Curing times were set at 90 days before testing. Finally, statistical analysis was carried out using Design Expert software with RSM, to optimize the mix by minimizing trials and analyzing the impacts of several variables, such as GP content and SF dose on strength. Regression analysis was utilized to create prediction models for strength based on experimental data. Furthermore, the optimized mix design was evaluated by redoing the experiments and

comparing the findings to the regression models' expected outcomes, ensuring that the intended mechanical properties of the SCM are consistently attained throughout multiple trials.

Table 1: Mix Proportion

Mix ID	GP Replacement (%)	SF Content (% by Volume)	Cement (kg/m³)	GP (kg/m³)	SF (kg/m³)
M1	0	0	5.2	0	0
M2	0	0.5	5.2	0	0.01
M3	0	1	5.2	0	0.052
M4	7.5	0	4.81	0.39	0
M5	7.5	0.5	4.81	0.39	0.01
M6	7.5	1	4.81	0.39	0.052
M7	15	0	4.42	0.78	0
M8	15	0.5	4.42	0.78	0.01
M9	15	1	4.42	0.78	0.052
M10	22.5	0	4.03	1.17	0
M11	22.5	0.5	4.03	1.17	0.01
M12	22.5	1	4.03	1.17	0.052

2.3 Testing Methods

2.3.1 Microstructural characterization

The chemical composition of processed GP was determined using X-ray Fluorescence (XRF) spectrometry at the Integrated Research Laboratories in Ibadan, Nigeria. This approach was used to detect and quantify the elemental oxides in the material, which provided important information for determining its potential as a supplementary cementitious material. SEM was used to study the surface morphology and internal structure of mortar after 7 days of curing. The samples were cleaned, dried, and trimmed to size before being mounted on conductive stubs and coated with gold or carbon. Imaging was carried out in vacuum at various magnifications. Observations focused on fiber-matrix bonding, pore distribution, and morphological changes. The analysis followed ASTM E1508 (2012) and was carried out at Integrated Research Laboratories, Ibadan. XRD was used to determine crystalline phases in the mortar mixes after 7 days using Rigaku D/Max-llllC X-ray diffractometer created by Rigaku Int. Corp. Tokyo, Japan in accordance with ASTM C1365-18. It was carried out at Integrated Research Laboratories, Ibadan, Nigeria.

2.3.2 Compressive strength

This compressive strength was conducted to evaluate the load-bearing capacity of mortar mixes containing SF and GP. The materials were thoroughly mixed and cast into standard cube molds, then compacted and cured for 90 days. The samples were taken out of the curing tank, and tested using a Universal Testing Machine (UTM) shown in Figure 2 at the University of Ilorin. Load was applied steadily until failure occurred, and the peak load sustained by each specimen was recorded. The test procedure conformed to BS EN 1015-11:2019 standards, ensuring accuracy and consistency.

2.3.3 Flexural strength

Flexural strength testing was conducted to assess the bending resistance of mortar mixes incorporating SF and GP (Figure 3). Specimens of 40 × 40 × 160 mm were prepared and cured. The test followed the procedures outlined in BS EN 1015-11 which prescribes methods for determining the flexural strength of hardened mortar. A three-point loading configuration was employed, where each prism was placed on two support rollers and subjected to a central load using UTM. The applied load was gradually increased until the specimen fractured, and the maximum load at failure was recorded.

Figure 2: Compressive Strength Test Setup

Figure 3: Flexural Strength Test Setup

3. RESULTS AND DISCUSSION

3.1 Characteristics of GP

The XRF data (Table 2) support the pozzolanic potential of the GP used. The SiO_2 concentration was 52.54%, and the total oxides SiO_2, Al_2O_3, and Fe_2O_3 amounted to 85.04%, exceeding the ASTM C618 minimum requirement of 70% for Class N pozzolans. These values represent the material's suitability as a pozzolan. Figure 4 shows strong peaks, indicating a primarily crystalline structure containing phases such as kaolinite, quartz, albite, and muscovite. The lack of a broad hump indicates low amorphous content, implying a clay-based or ceramic origin rather than soda-lime glass. The SEM image of the waste material, illustrated in Figure 5 at a magnification of 10,000× and an accelerating voltage of 15 kV, displays a highly textured and uneven surface morphology. The particles exhibit jagged contours, layered formations, and notable internal voids. The appearance of sheet-like and plate-shaped elements implies the existence of thermally processed clay-based minerals, such as kaolinite or illite, which are commonly associated with calcined pozzolanic substances. These microstructural traits contribute to an expansive surface area, enhancing the material's reactivity with calcium hydroxide to form additional calcium silicate hydrate (C–S–H) during the cement hydration process. The irregular shape and porous composition of the particles also support improved matrix compaction and enhanced long-term performance in cement-based applications.

Table 2: Chemical Composition of GP

Component	GP (%)
SiO_2	52.54
Al_2O_3	28.85
Fe_2O_3	3.65
MnO	0.01
CaO	1.94
P_2O_5	-
K_2O	0.95
TiO_2	1.17
MgO	0.08
Na_2O	0.05
$SiO_2 + Al_2O_3 + Fe_2O_3$	85.04

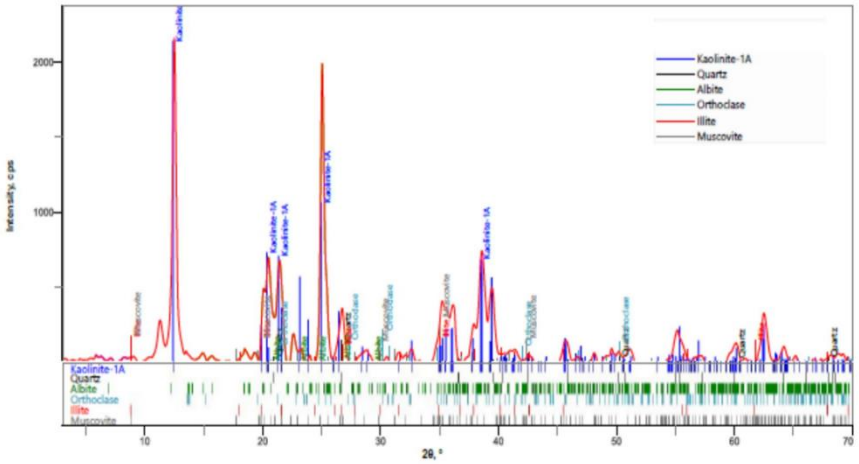

Figure 4: XRD Pattern of Glass Powder

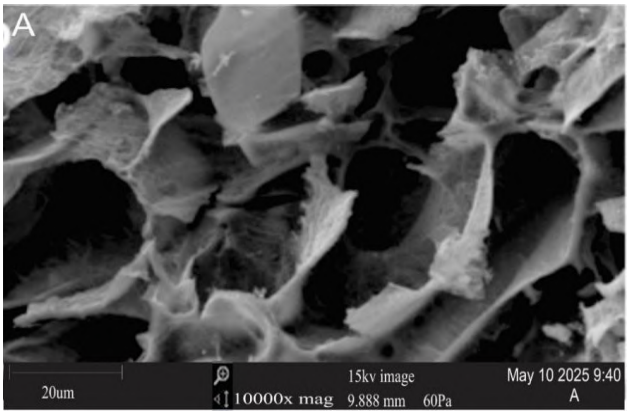

Figure 5: SEM Image of Glass Powder

3.2 XRD Analysis of Mortar

The XRD pattern (Figure 6a) of sample M1, analyzed qualitatively using the 2nd differential method, shows a 2θ range from 20° to 70° with peak intensities reaching approximately 400 cps and a typical peak width of 0.065°. The major crystalline phases identified include Quartz (Q) with sharp, intense peaks around 21°, 26.5°, 31°, 36°, and 50°, indicating its dominance; Kaolinite (K) with peaks around 30°, 38°, and 42°; Calcium Oxide (Ca) with a peak near 29°; and Iron Oxide (Fe_2O_3) showing multiple peaks at 38°, 46°, 52°, and 60°. Additional minerals such as Mica (M), Smectite (Sm), and Illite (I) were observed at various angles, confirming the presence of natural clay-related components. A broad amorphous hump around 20° - 25° likely corresponds to C-S-H gel, indicating partial hydration. Overall, the composition shows a mix of crystalline and amorphous phases, indicating that the mortar powder is a cementitious material made up of quartz, aluminosilicate clays, calcium compounds, and iron oxides, making it suitable for construction applications due to its pozzolanic potential.

The XRD pattern (Figure 6b) of sample M2 containing 0.5% SF shows both crystalline and amorphous phases throughout a 2θ range of 5° to 75°, with peak intensities exceeding 1200 cps and an average peak width of 0.065°. Quartz (Q) is the dominating mineral phase, with prominent peaks at 21°, 27°, 31°, 39°, and 50°, indicating a highly crystalline siliceous matrix. Other prominent elements are kaolinite (K) and mica (M), which have separate peaks at 35°, 45°, and 60°, indicating the presence of aluminosilicate and clay minerals. Iron oxide (Fe) is identified with peaks at 15°, 33°, and 55°, whereas calcium oxide (Ca) emerges at 25° and 38°, indicating cementitious activity. Notably, Zeolite (Z) is also identified, especially

around 45° and 70°, indicating possible pozzolanic reactivity or residue from SF treatment. A broad hump below 15° may indicate the presence of amorphous hydration products like C-S-H.

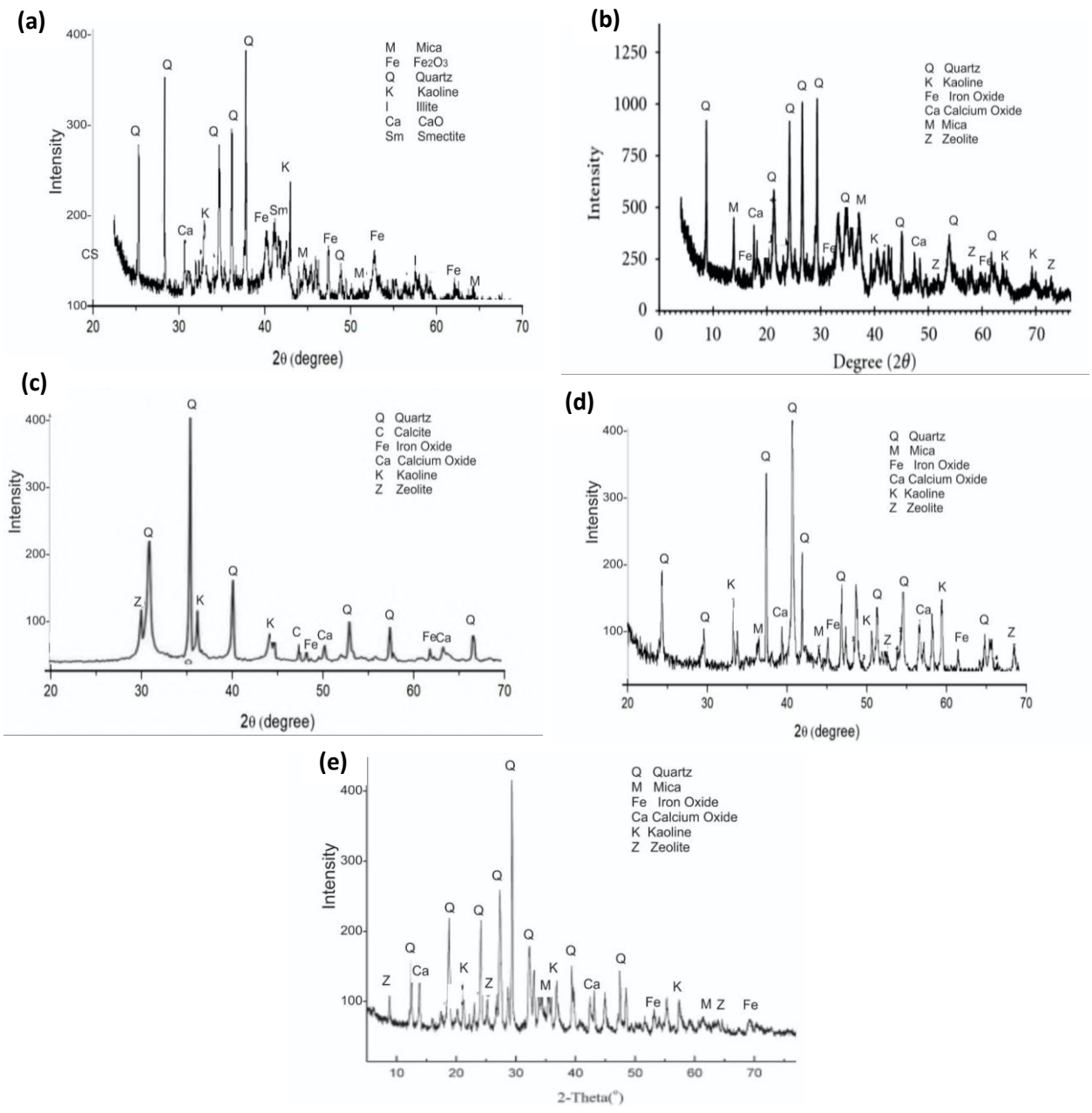

Figure 6: XRD pattern of (a) M1 (b) M2 (c) M3 (d) M4 (e) M7

The XRD pattern (Figure 6c) of sample M3, incorporating 1% SF, reveals a predominantly crystalline profile within a 2θ range of 20° to 70°, with a peak intensity slightly above 400 cps and a typical peak width of 0.065°. Quartz (Q) remains the dominant mineral phase, marked by sharp, intense peaks around 27°, 31°, 42°, 50°, and 68°, confirming a siliceous base structure. The presence of Kaolinite (K) and Zeolite (Z) is also evident from peaks near 35° and 29°, indicating retained aluminosilicate and pozzolanic components. Iron Oxide (Fe) and Calcium Oxide (Ca) appear with lower intensities between 45° and 60°, along with a minor Calcite (C) peak around 48°, suggesting carbonation or secondary calcite formation. Compared to

the 0.5% SF sample, the 1% SF addition appears to slightly reduce the intensity of some minor phases while maintaining the integrity of the main crystalline components. This may indicate improved matrix homogeneity and enhanced internal curing from the fiber interaction, with potential benefits for durability and microstructural refinement.

The XRD pattern (Figure 6d) of the sample M4 containing 7.5% GP reveals dominant peaks corresponding to quartz (Q), indicating it is the major crystalline phase present, while kaolinite (K), mica (M), calcium oxide (Ca), iron oxide (Fe), and zeolite (Z) appear as minor phases. The strong intensity of the quartz peaks, particularly around 26.6°, 36.5°, and 50° 2θ, confirms its abundance, whereas kaolinite and mica are observed through smaller peaks near 25°, 32°, and 38°. The presence of calcium oxide, detected around 34°, 47°, and 60°, may suggest incomplete hydration or residual lime, and iron oxide, seen near 45° and 61°, could be derived from cement or impurities in the GP. Zeolite, appearing around 49° and 67°, might be a product of pozzolanic reactions or present as an additive. Although the GP itself is amorphous and does not produce distinct peaks, its presence is implied through the potential formation of amorphous C-S-H gel and zeolitic phases, indicating that pozzolanic activity may be occurring. Overall, the diffraction pattern suggests a highly crystalline matrix dominated by quartz, with supplementary phases reflecting the complex interactions within the mortar modified with 7.5% GP.

The XRD pattern (Figure 6e) of sample M7 containing 15% GP exhibits a strong crystalline structure dominated by quartz (Q), as evidenced by the prominent peaks particularly around 21°, 27°, and 50° 2θ, indicating quartz as the major mineral phase. Minor peaks corresponding to kaolinite (K), mica (M), calcium oxide (Ca), iron oxide (Fe), and zeolite (Z) are also identified, suggesting the presence of secondary mineral phases. The peak intensity of calcium oxide, observed near 13° and 34°, reflects possible unreacted lime or hydration products, while the presence of zeolite around 9°, 24°, and 60° may imply pozzolanic transformation associated with the added GP. The detection of iron oxide and mica at lower intensities near 47° and 65° supports their role as trace components. Although the GP itself is amorphous and does not contribute sharp peaks, its integration appears to have influenced the formation of zeolite and possibly enhanced the amorphous phase fraction, supporting ongoing pozzolanic activity. Overall, the pattern suggests a crystalline framework largely composed of quartz, with mineralogical evidence indicating that the addition of 15% GP contributes to secondary phase development through pozzolanic reactions.

3.3 SEM Analysis of Mortar

The SEM image (Figure 7a) of sample M1, captured at a high magnification of 9,000x using a scanning electron microscope (SEM) operating at 15 kV, displays irregularly shaped particles typical of crushed or ground materials, with textures ranging from angular to slightly rounded depending on processing methods. The scale bar (100 µm) indicates a mix of fine and coarser particles, while surface features such as roughness, pores, or fractures are likely visible, reflecting the brittle nature of cementitious materials. The SEM image (Figure 7b) captures sample M2 reinforced with 0.5% SF, imaged at 6,000x magnification under 15 kV, where the 100 µm scale bar reveals both the granular mortar matrix and the distinctive fibrous structures of the SF reinforcement. The mortar particles exhibit irregular shapes and surface textures typical of cementitious materials, while the SF appear as elongated strands either well-bonded to or partially detached from the matrix, highlighting potential interfacial behavior critical for composite performance.

Figure 7c shows the microstructure of sample M3 containing 1% SF at 5000x magnification. The micrograph reveals a heterogeneous and porous matrix with a mixture of fine and coarse particles. The surface appears rough and irregular, with numerous voids and micro-cracks throughout the structure. These features suggest the influence of SF in disrupting the compactness of the mortar matrix, possibly due to its organic nature and interaction with the hydration process. The presence of spherical and sub-angular particles indicates remnants of unhydrated cement grains or reaction products, while the loosely bound clusters and porous regions point to reduced densification, likely attributed to the inclusion of SF. Overall, the image suggests that the addition of 1% SF contributes to a more open and porous microstructure, which can influence the mechanical and durability properties of the mortar.

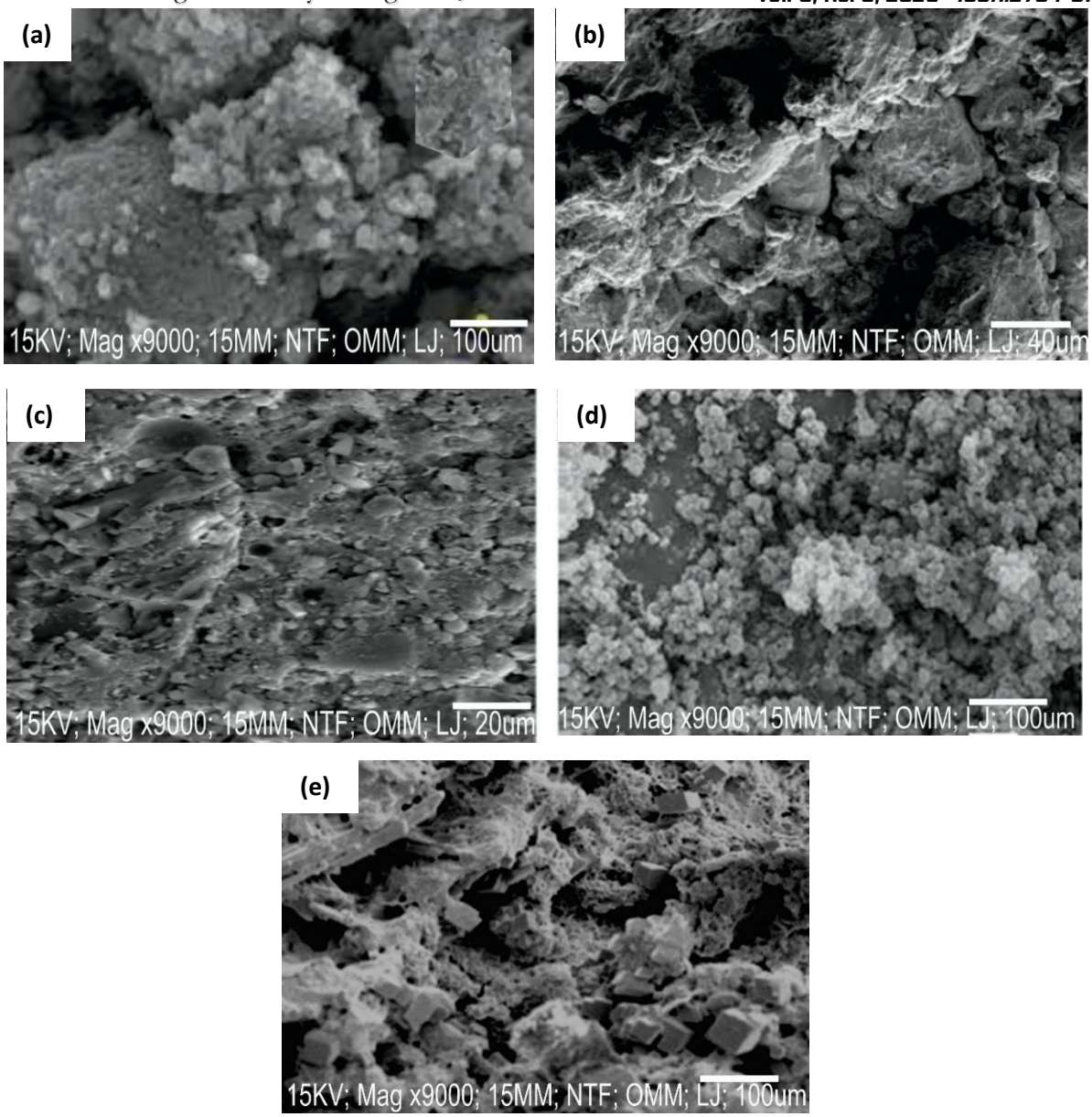

Figure 7: SEM Image of (a) M1 (b) M2 (c) M3 (d) M4 (e) M7

The SEM image (Figure 7d) reveals the microstructure of sample M4 modified with 7.5% GP, captured at 9,000x magnification under 15 kV, where the 100 µm scale bar highlights the composite's distinct features. The GP particles appear as smooth, rounded inclusions contrasting sharply with the irregular, angular morphology of the cementitious matrix, creating a clearly defined interfacial boundary that suggests limited chemical interaction at this scale. This heterogeneous distribution of glass particles within the mortar matrix likely enhances particle packing density while contributing to pozzolanic reactivity, potentially improving the material's long-term strength and durability characteristics.

The SEM image (Figure 7e), under optimized imaging conditions (15 kV accelerating voltage, 8.5 mm working distance, and 70 Pa chamber pressure), reveals the microstructure of sample M7 containing 15% additive at 6,000x magnification, where the 21.0 µm horizontal field width and 15 µm scale marker highlight significant microstructural modifications. The high additive content appears as distinct phases

uniformly distributed throughout the cementitious matrix, with clearly visible interfacial zones that exhibit either strong bonding indicative of effective stress transfer or potential reaction rims suggesting pozzolanic activity, while the mortar matrix itself displays characteristic angular particles whose packing density and pore structure appear substantially altered by the additive incorporation.

3.4 Compressive Strength

The 3D surface plot in Figure 8 illustrates the relationship between the 90 days compressive strength of mortar (in N/mm²) and the combined effects of GP and SF content. The increase in compressive strength observed with the incorporation of GP up to 7.5% can be attributed to its high silica and alumina contents, which enhance pozzolanic activity and contribute to the formation of additional C–S–H and C–A–S–H gels. This reaction refines the pore structure and strengthens the interfacial transition zone (ITZ), leading to a denser and more cohesive matrix. The XRD results support this mechanism, revealing the development of weak amorphous humps and zeolitic phases indicative of secondary hydration. Correspondingly, SEM images show a compact microstructure with reduced voids and well-bonded particles in the 7.5% GP mix, which aligns with the peak compressive strength recorded. However, beyond 7.5% GP replacement, a decline in strength was noted, likely due to excess GP diluting cement content and increasing unreacted particles, as reflected in the more amorphous microstructure observed in the XRD and SEM analyses. The inclusion of 0.5% SF further enhanced compressive strength through improved stress distribution and internal curing, as the fibers retained moisture that prolonged pozzolanic reactions. At 1% SF, however, SEM micrographs indicated fiber clustering and void formation, which hindered matrix compaction and caused a slight strength reduction.

3.5 Flexural Strength

After 90 days of curing, the 3D relationship between flexural strength, SF and GP contents shows a synergistic influence on the mortar performance (Figure 9). Flexural strength followed a similar trend to compressive strength, with the optimum performance achieved at 7.5% GP and 0.5% SF. The increase is primarily linked to the combined effects of improved matrix densification and effective fiber–matrix bonding. XRD patterns for these mixes revealed new reaction products and reduced crystalline peaks, signifying enhanced pozzolanic reactivity that strengthens the ITZ and improves load transfer efficiency. SEM observations confirmed the presence of uniformly dispersed fibers bridging microcracks and creating a cohesive, compact surface morphology. This microstructure accounts for the superior flexural strength and reduced crack propagation. Conversely, at higher GP or SF contents, excessive replacement or fiber entanglement introduced weak zones and microvoids, as evident in the micrographs, thereby reducing flexural capacity. The integrated microstructural evidence thus validates the mechanical test results, confirming that the synergy between pozzolanic reaction (from GP) and fiber reinforcement (from SF) governs the enhanced strength behavior of the modified mortars. The addition of SF increased flexural strength by bridging microcracks and improved the toughness and ductility of the composite, corroborating the findings of Zhou *et al.* (2024). Simultaneously, the inclusion of GP, due to its pozzolanic reactivity, stimulated further cementitious processes, resulting in a denser microstructure and increased compressive strength, as demonstrated by Maraghechi *et al.* (2014). Together, these materials considerably improved the mortar's flexural behaviour, with both components having complimentary roles in matrix strength.

3.6 Model Equation

A linear regression model was created to assess the compressive strength (in N/mm²) of mortar using GP and SF content. The last expression in terms of real factor levels is shown in equation 1. A First-order regression model was formulated to predict the flexural strength (in N/mm²) of mortar as a function of GP and SF content. The final expression in terms of actual factor levels is shown in equation 2.

$$\text{Compressive Strength} = 17.28 - 0.236 \cdot GP + 0.791 \cdot SF \quad (1)$$

$$\text{Flexural Strength} = 6.69 - 0.043 \cdot GP + 0.525 \cdot SF - 0.044 \cdot (GP \times SF) \quad (2)$$

Where, GP = Glass Powder (%) and SF = Sisal Fiber (%)

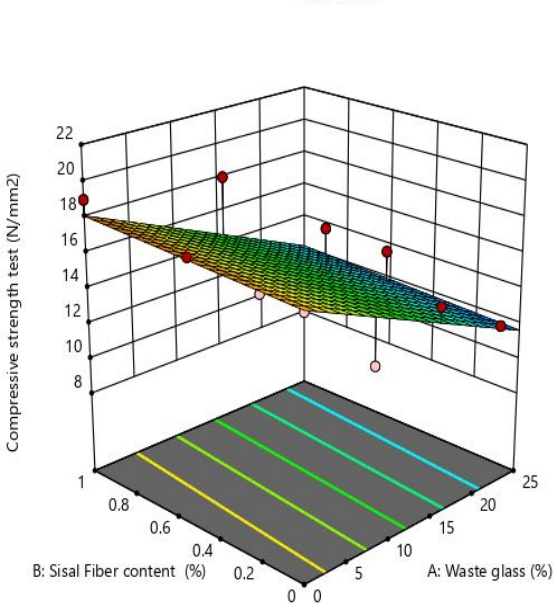

Figure 8: 3D Plot for Compressive Strength

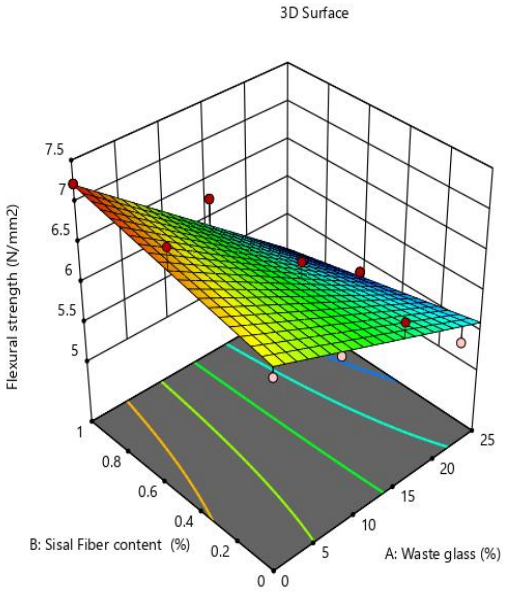

Figure 9: 3D Plot for Flexural Strength

3.7 Validation

The validation results in Table 3 indicate that the developed models for both compressive strength and flexural strength of the mortar are statistically robust and highly reliable. For compressive strength, the high coefficient of determination (R^2 = 0.909) shows that 90.9% of the variation in the experimental data is explained by the model, suggesting a strong correlation between the observed and predicted values. The adjusted R^2 = 0.8908, which accounts for the number of input factors, confirms that the model is efficient and not over-parameterized. Furthermore, the predicted R^2 = 0.8454 demonstrates strong predictive power when applied to unseen data, while the adequate precision value of 17.441—well above the minimum desirable threshold of 4—indicates a high signal-to-noise ratio and sufficient model discrimination.

Similarly, for flexural strength, the R^2 = 0.8955 shows that 89.55% of the data variability is effectively captured, and the adjusted R^2 = 0.8606 suggests good model generalization without overfitting. The predicted R^2 = 0.7856, though slightly lower than the adjusted R^2, remains within an acceptable range, confirming reliable external predictive performance. The adequate precision of 14.3191 again signifies a strong model signal relative to random error. Overall, these statistics indicate that both models have excellent fitting and predictive accuracy, making them reliable tools for optimizing mortar composition using GP and SF. However, the slightly lower predicted R^2 values compared to the adjusted R^2 suggest minor variability that could arise from experimental noise, material heterogeneity, or unmodeled interaction effects. This implies that while the models are highly predictive within the tested range, extrapolation beyond these experimental conditions should be approached with caution. Nonetheless, the models provide a solid statistical foundation for developing eco-efficient, high-performance SCM.

Table 3: Results Validation

	Compressive strength	Flexural strength
R^2	0.909	0.8955
Adjusted R^2	0.8908	0.8606
Predicted R^2	0.8454	0.7856
Adeq Precision	17.441	14.3191

3.8 Optimization

The optimization of the mortar mix design in Figure 10 shows that incorporating approximately 7.5% GP and 0.5% SF results enhanced mechanical properties, including a FS of 6.46 MPa and a CS of 15.89 MPa, all while achieving the highest possible desirability score of 1.000, indicating an ideal balance of performance and sustainability.

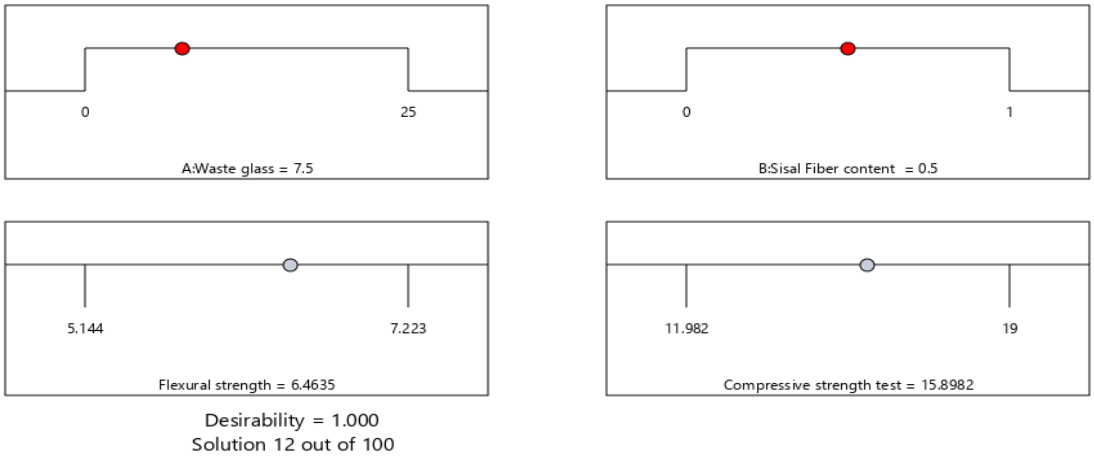

Figure 10: Optimized Result

4. CONCLUSION

This study employs CCD in Design Expert software to optimize SCM mixes with GP replacing cement at 0–22.5% and SF added at 0–1% by volume. The compressive strength declined with higher GP content but improved with the inclusion of SF due to its crack-bridging effect. Notably, flexural strength exhibited a synergistic increase when both materials were combined. XRD and SEM analyses revealed quartz as the dominant crystalline phase. GP contributed to the formation of amorphous C-S-H, while SF enhanced pozzolanic activity through zeolite formation. Although higher SF content (1%) increased porosity, it significantly improved fiber–matrix interfacial bonding. The optimal blend was determined to be 7.5 % GP and 0.5% SF, achieving enhanced strength characteristic. This combination yielded a desirability score of 1.000, indicating optimal performance.

References

Asonibare, I., Abdulwahab, R., & Adisa, M. (2025). Effect of pulverized burnt clay waste as a partial replacement of cement on the fresh and mechanical properties of concrete. *Discover Concrete and Cement*, 1(1), 1–15. https://doi.org/10.1007/S44416-025-00016-6

ASTM (American Society for Testing and Materials) (2012). Standard guide for quantitative analysis by energy-dispersive spectroscopy. *ASTM E1508.* ASTM Standards.

Bentlemsan, N., Yahiaoui, W., & Kenai, S. (2023). Strength and durability of self-compacting mortar with waste marble as sand substitution. *Case Studies in Construction Materials*, 19. https://doi.org/10.1016/j.cscm.2023.e02331

Byrne, C. L. (2014). A first course in optimization. https://doi.org/10.1201/b17264

de Souza, M. H. B., Silva, L. R. R., Ribeiro, V. A. dos S., Gonçalves, P. C., Melo, M. de L. N. M., Gomes, C. E. M., & dos Santos, V. C. (2023). Influence of superabsorbent polymer in self-compacting mortar. *Buildings*, 13(7). https://doi.org/10.3390/buildings13071640

Hammat, S., Menadi, B., Kenai, S., Khatib, J., & Kadri, E. H. (2021). Properties of self-compacting mortar containing slag with different finenesses. *Civil Engineering Journal*, 7(5). https://doi.org/10.28991/cej-2021-03091694

Horsakulthai, V. (2021). Effect of recycled concrete powder on strength, electrical resistivity, and water absorption of self-compacting mortars. *Case Studies in Construction Materials*, 15. https://doi.org/10.1016/j.cscm.2021.e00725

Maraghechi, H., Maraghechi, M., Rajabipour, F., & Pantano, C. G. (2014). Pozzolanic reactivity of recycled glass powder at elevated temperatures: Reaction stoichiometry, reaction products and effect of alkali activation. *Cement and Concrete Composites*, 53. https://doi.org/10.1016/j.cemconcomp.2014.06.015

More, F. M. D. S., & Subramanian, S. S. (2022). Impact of fibres on the mechanical and durable behaviour of fibre-reinforced concrete. *Buildings*, 12(9). https://doi.org/10.3390/buildings12091436

Naran, J. M., Gonzalez, R. E. G., del Rey Castillo, E., Toma, C. L., Almesfer, N., van Vreden, P., & Saggi, O. (2022). Incorporating waste to develop environmentally-friendly concrete mixes. *Construction and Building Materials*, 314. https://doi.org/10.1016/j.conbuildmat.2021.125599

Nécira, B., & Abadou, Y. (2021). Properties of self-compacting mortar made with various mineralogical sources different types of sands and fillers. *World Journal of Engineering*, 18(6), 861–869. https://doi.org/10.1108/WJE-10-2020-0483

Olofinnade, O. M., Ndambuki, J. M., Ede, A. N., & Booth, C. (2017). Application of waste glass powder as a partial cement substitute towards more sustainable concrete production. *International Journal of Engineering Research in Africa*, 31. https://doi.org/10.4028/www.scientific.net/JERA.31.77

Olorunfemi, K. O., Odeyemi, S. O., & Adisa, M. A. (2025). Development of high-performance concrete using guinea corn and rice husk ashes as replacement for silica fume. *Next Sustainability*, 6, 100203. https://doi.org/10.1016/J.NXSUST.2025.100203

Rodier, L., & Savastano, H. (2018). Use of glass powder residue for the elaboration of eco-efficient cementitious materials. *Journal of Cleaner Production*, 184. https://doi.org/10.1016/j.jclepro.2018.02.269

Sara, B., Mhamed, A., Otmane, B., & Karim, E. (2023). Elaboration of a self-compacting mortar based on concrete demolition waste incorporating blast furnace slag. *Construction and Building Materials*, 366. https://doi.org/10.1016/j.conbuildmat.2022.130165

Tijani, M. A., Opadotun, K. J., Raifu, W. O. and Ajagbe, W. O. (2025). Effect of binary blend of sorghum husk ash and glass powder as partial replacement of cement in pervious concrete production. *Proceedings of the Sustainable Construction in Africa (SCA25) Conference*, 1 – 10. https://www.epfl.ch/labs/lmc/

Zhou, H., Wu, J., Wang, X., Song, T., & Wang, Y. (2024). Thickness effect of engineered cementitious composites subjected to quasi-static and dynamic tension. *Construction and Building Materials*, 421. https://doi.org/10.1016/j.conbuildmat.2024.135583.